$$V_{dc} = \left(V_{mp} \times f_{temp\_vmp} \times N_s\right) \times \left[1 + k \ln\left(\frac{G}{1000}\right)\right] \quad (3)$$

where V_{dc} is the maximum power condition output of voltage of the PV array at STC. Meanwhile, the constant, k is to get the desired point and obtained by using curve fitting techniques. A temperature factor is indicated in equation (4):

$$f_{temp\_vmp} = 1 + \left[\left(\frac{\gamma_{vmp}}{100}\right) \times \left(T_m - 25\right)\right] \quad (4)$$

where Y_{vmp} is defined as temperature coefficient for power in %/^{o}C^{-1} or %/K. In certain situations where the PV modules datasheet only provides temperature coefficient for voltage at open circuit condition, Y_{voc}. It can be considered Y_{vmp} is equal to Y_{voc}. N_s represent the number of PV modules connected in series. Equation (5) predicts the DC current:

$$I_{dc} = I_{mp} \times f_{temp\_pmp} \times N_P \times f_{dirt} \times f_{mm} \times \frac{G}{1000} \quad (5)$$

where I_{mp} is the current at maximum power of PV array at STC and total number of PV strings that connected in parallel is represented as N_P. Whereas, f_{temp_imp} is the temperature factor which can be determined as equation (6):

$$f_{temp\_vmp} = 1 + \left[\left(\frac{\gamma_{imp}}{100}\right) \times \left(T_m - 25\right)\right] \quad (6)$$

DC current can also be predicted using equation (7) with reference to equation (1) and (3):

$$I_{dc} = \frac{P_{dc}}{V_{dc}} \quad (7)$$

The inverter efficiency can be concluded using equation (8) where AC power could be extracted from logged data:

$$\eta = \frac{P_{ac}}{P_{dc}} \quad (8)$$

The overall system performance is determined by the performance parameters through energy production, solar resources and the overall effect of the system loss. These parameters are the PV energy yield, specific yield and performance ratio.

The AC energy output of the PV system for both actual and predicted data is calculated from the equation (9):

$$E_{sys} = \sum P_{ac} \times \frac{t}{60} \quad \text{(kWh)} \quad (9)$$

where P_{ac} is the actual and predicted AC power meanwhile t is refer to sampling time of PV system.

The net AC energy output per kWp of PV array, known as specific yield, Y_f is the relationship between the total energy output from inverter and the size of PV array. To provide the same energy, specific yield represents the number of hours necessary for PV array operating at rated power. To normalize the energy produced with respect to the size of the PV system, the specific yield can be resolved using equation (10):

$$Y_f = \frac{E_{sys}}{P_{array\_stc}} \quad \text{(kWh kWp}^{-1}\text{)} \quad (10)$$

Performance ratio, *PR* expects the overall effect of losses in efficiency inverter rated output, mismatch and other losses when switching from DC power to AC power. Based on case studies, each year the *PR* will be reported and this is very useful to identify any incidents of component failure. According to a source [9], based on Malaysia climate, *PR* acceptable value should be more than 70%. For actual and predicted data, the performance ratio *PR* is determined by the equation (11).

$$PR = \frac{E_{sys}}{E_{ideal}} \quad (11)$$

where E_{ideal} is the PY array at STC ideal energy output which could be drawn from equation (12) [9]:

$$E_{ideal} = P_{array\_stc} \times PSH_{period} \quad (12)$$

where PSH_{period} is the peak sun hour value for the particular tilt angle over the period of occurrence in hours (h).

To measure the fitness of the model, the coefficient of determination, R^2 is proposed. This coefficient is described as follows:

$$Y = mX + C \quad (13)$$

In this study, R^2 measures the goodness of fit in the sense of comparing Actual values and Predicted values. R^2 acquire values between 0(extremely poor fit) and 100% (perfect fit). In general, the higher R^2, the better model fits to the data [10].

Equation (14) shows the calculation of the percentage error to compare the prediction value with an actual value. It will prove how close the prediction (manufacturer value) was to the actual value [11].

$$Error = \sum\left(\frac{\text{Prediction} - Actual}{Actual}\right) \times 100\% \quad (14)$$

III. METHODOLOGY

This study is divided into two characteristics; the mathematical approach in calculation of actual and predicted data and the visual inspection. Through visual inspection, the assessments are described as in Table I.

Figure 1 shows the system installed that was installed in 2004, and the details of the PV array are shown in Table 2.

Table 1. Assessment procedures conducted on modules

Assessment	Objective
Visual inspection	Inspect PV module visually
IV curves	Test electrical performance

A. PV panel

Fig. 1 PV systems installed

Table 2. Characteristics of the PV array

Ratings	Value
Manufacturer	SUNTECH
Model	STP160S-24/Ac
Type of PV technology	Monocrystalline
Nominal peak power rating	160W
Number of PV modules	7
Peak PV array capacity	1120Wp
Rated maximum power voltage of PV module	34.4V
Number of PV strings	1
Number of parallel PV strings	7
Rated maximum power voltage of PV array	34.4V

B. Inverter

A single grid-connected inverter model Solivia 3.3TR is connected to the utility grids show in Fig. 1. The characteristics of the inverter are as follows (Table 3):

Apart from the PV array and inverter, the system also consists of other balance of system components such as fuses and circuit breakers. Two temperature sensors and an irradiance sensor had been used to record the required climatic parameters for the performance monitoring. These sensors were then connected to a data logger called Solar Log. The irradiance sensor was used to obtain the solar irradiance in-plane of array (POA) The temperature sensors were used to obtain the ambient temperature and PV module temperature. These climatic data were recorded at a five minute interval. These data were accessed from the Solar Log data logger. The results presented in this paper were 8 consecutive days of full monitoring.

Fig. 2 Inverter

Table 3. Characteristics of Inverter

Ratings	Value
Nominal DC input voltage (V)	125
DC input range (V)	150-450
Maximum DC input voltage (V)	540
Maximum current (A)	24
Efficiency (%)	96

Table 3. Characteristics of Inverter

Table 4. Modules Evaluated With Performance Parameters at STC

Ratings	Value
Module	STP160S-24/Ac
I_{sc} (A)	5
V_{oc} (V)	43.2
P_{max} (W)	160
I_{mpp} (A)	4.65
V_{mpp} (V)	34.4

Table 4 shows the value of I_{sc}, V_{oc}, P_{max}, I_{mpp} and V_{mpp} at STC. STC refers to Standard Test Conditions, 1000 W/m^2 irradiance, 25 ^{o}C module temperature and Air Mass 1.5 global spectrum. Table IV shows these measurements were used as a baseline for future reference in studying the

influence of temperature and irradiance, and for comparison to measurements obtained during subsequent periodic assessments. Visual inspection of the modules has revealed some defects during the initial assessment.

In this study, electrical measurements were performed to test the module output. The IV characteristics were measured with a TRI-KA the mobile IV curve tracer and from these the temperature and irradiance adjusted efficiency, fill factor and maximum power under approximately AM1.5 conditions were calculated. These were then compared with the manufacturer's specification. This allows the researcher to determine if the defects identified under visual inspection were detrimentally affecting the module output. The shape of the IV curve can also provide some information of whether there are any problems within the module.

Infrared photographs of the solar module were taken using a FLUKE Ti125 IR camera (refer Figure 3 and Table 5). The measurement were taken while the panel is under load and exposed to ambient lighting on a clear day. The infrared images allow the identification of possible hot spots and cracks within the module. This inspection allows the detection of defects which are not visible with a naked eye. These include cracked or broken cells, hot spots in the cells or their connections and soldering, non active cells or regions which do not contribute to photogeneration and failures in bypass diodes [12].

Table 5. Detailed Specification of Thermal Imager

Ratings	**Details**
Camera model	Fluke Ti125 Thermal Imager
IR resolution (FPA size)	160 x 120 FPA Uncooled Microbolometer
Spectral band	7.5 µm to 14 µm (long wave)
NETD (Thermal sensitivity)	≤ 0.10 °C at 30 °C target temp (100 mK) 0.10 °C at 30 °C target temp (100 mK)
Temperature measurement range (not calibrated below -10 °C)	-20 °C to +350 °C (-4 °F to +662 °F)
Temperature measurement accuracy	± 2 °C or 2 % (at 25 °C nominal, whichever is greater)
Minimum IR focus distance	15.25 cm (6 in)

Figure 3 FLUKE Ti125 IR camera the thermal imager equipment for thermographic techniques [13]

IV. RESULTS AND DISCUSSION

A. Visual Inspection

In this work, there are many types of defects that appear on PV modules were analysed. These visually identify the different types of defects that were found in the measured modules. Examples of some defects are shown in Table VI. There are also some defects shown by using infrared photography. The main characteristics of the defects can be described as follows:

- slight chalking backsheet
- degraded wires
- weathered junction box
- minor corrosion and degraded frame
- light discoloration
- corrosion on gridlines of the modules

Those results correspond to what had been obtained in Table 6

Table 6. Visual Inspection of PV Systems

Components	**Defect**	**Image**
Glass cover	Snails track Bird dropping	
Backsheet	Slight chalking	
Wires	Pliable but degraded	

Junction Box	Physical: Weathered Adhesive: Pliable but degraded	
Frame	Physical: Minor corrosion Adhesive: Degraded	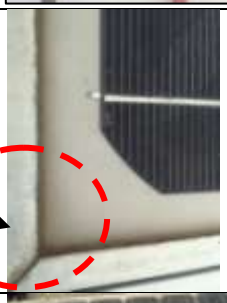
Metallization	Gridlines: Light discoloration Cracking Busbars: Light discoloration Cell interconnect ribbon: Light discoloration String interconnect: Light discoloration	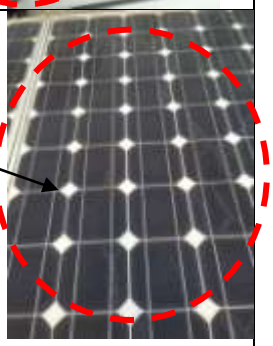 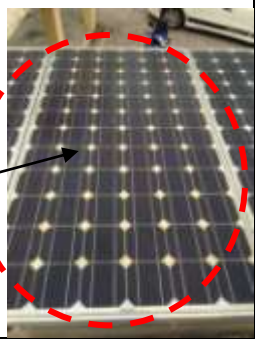

Table VI above showed the visual degradation of several components such as backsheet, wires, junction box and metallization. According to [14], delamination was a common problem and occurred more frequently in hot and humid climate, as what had been obtained in this study [15]. Besides, module discoloration was most probably due to humidity where Malaysia was also one of high humidity country. According to [16], ageing effects might be due to external factors such as overlaying dust, dirt, bird droppings, surrounding vegetation or fence, shading or strong winds which might affect the modules.

B. Module Temperature

The module temperature of PV panel photographs as taken by FLUKE Ti125 thermal camera have shown there are several spots on the PV modules have higher temperature compared to the overall surface. Figure 4 to 6 show the details.

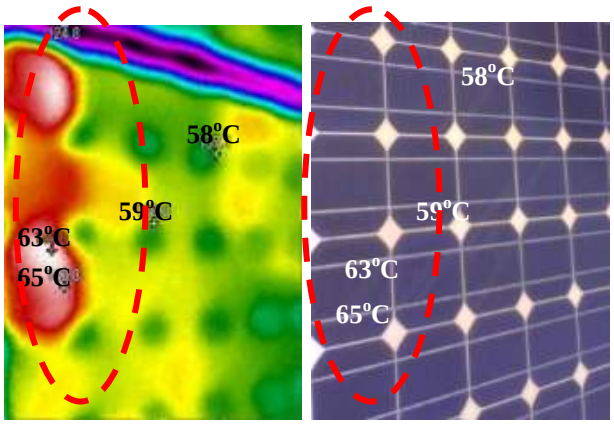

Figure 4 PV module with discoloration defect shows slightly higher temperature on certain spots

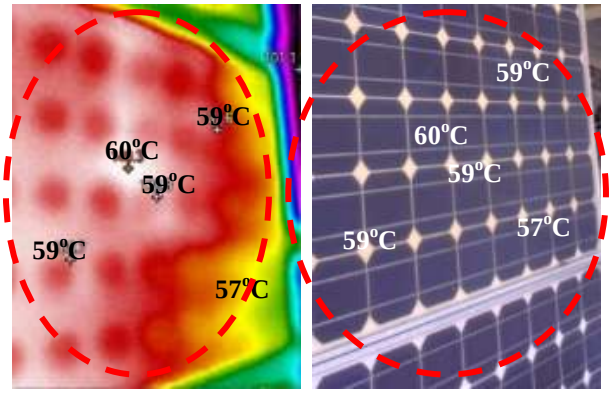

Figure 5 PV module with discoloration defect shows mostly higher temperature on certain spots

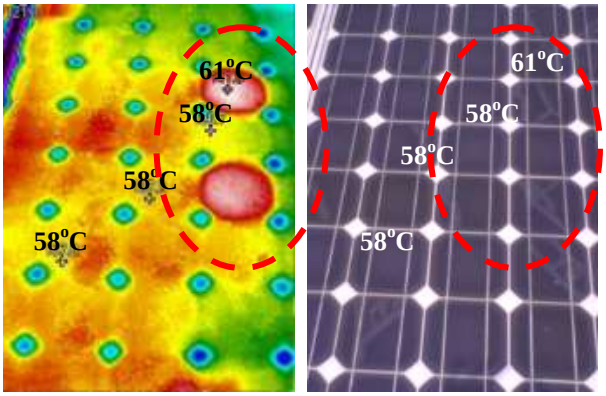

Figure 6 PV module with snails track show slightly higher temperature on certain spots

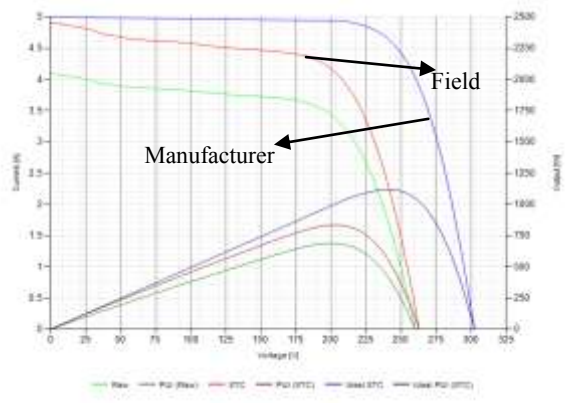

Figure 7 IV curve graphs from TRI-KA measurement

Table 7 shows the value extracted from TRI-KA the mobile IV curve tracer. The data have shown that the errors contribution mostly from V_{mpp} and P_{mpp}. The lost value of V_{mpp} is almost 39.3 V which is 19.5%. The value shows that the lost was almost likely consumed a single module where a single module contributes 34.4 V V_{mpp}. In contrast, the P_{mpp} loss value was 285 W most likely 2 modules had faults. To conclude, the system might have lost several modules due to fault or each modules have contributes faults as the total of power lost was high. The field factor (FF) also reaffirm the lost about 13.85% compared to the manufacturer value caused by the faulty modules.

Table 7. The Comparison Values Between the Field Data and the Manufacturer Data. Results After 12 Years of Installations

Ratings	**Field (Red line)**	**Manufacturer (Blue line)**	**Percentage different (%)**
I_{sc} (A)	4.894	5	2.17
I_{mpp} (A)	4.146	4.65	12.16
V_{oc} (V)	263.3	302.4	14.85
V_{mpp} (V)	201.5	240.8	19.5
P_{mpp} (W)	835	1120	34.13
FF	0.65	0.74	13.85

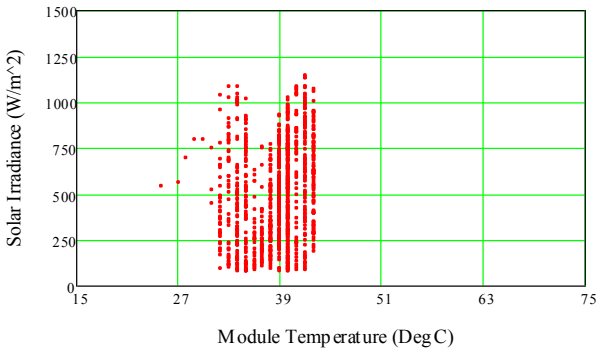

Figure 8 Module temperature using temperature sensor data logger

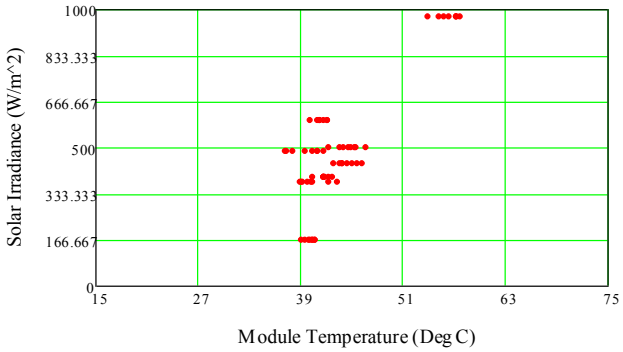

Figure 9 Module temperature using thermal imager

It can be seen that the module temperature detected from thermal imager were slightly higher compared to the module temperature detected using temperature sensor. Figure 8 and 9 stated that the value using thermal imager were around 37°C to 60°C compared to the values taken from temperature sensor range only within 27°C to 42°C. The difference between these values are each PV modules thermal image were taken using the thermal camera, hence the average values of the temperature was the contribution of every single PV modules on the systems compared to values from temperature sensor. It is because only one sensor placed on the PV system as represented for the whole systems.

C. The performance of PV systems

1) *Performance of PV array*: The performance of PV array is illustrated in Figure 10. In Figure 10, the AC output power generated by the PV modules is linearly dependent on the in-plane irradiance, except for lower irradiance values. At irradiance values lower than 80 W/m^2, the output power was found to be approximately zero. As the irradiance increases, the AC power generated by PV array correspondingly increases.

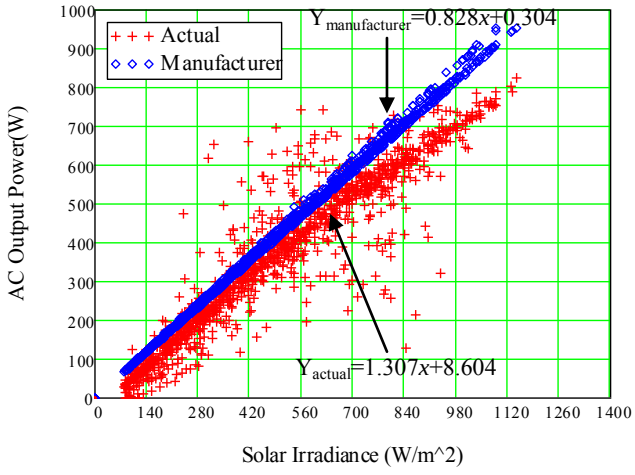

Figure 10 The relationship between the output power of PV array and the in-plane irradiance

The comparison between actual and manufacturer simulation results of output AC power produced from inverter are presented in Table 8. As refer to the regression line, the actual and manufacturer of AC Power is represent

as dependent variables, *y* and independent variables which is *x* indicate of solar irradiance. It can be seen the linear trend line of actual data is slightly lower compared to predicted trend line. The result of this analysis also shows a significant increase in AC power as function of solar irradiance increased. It can be seen that the percentage error is observed 13.2%, which the value of actual data has been interrupted by the faulty modules.

TABLE 8. Determination Coefficient, R2 and Percentage Error

	The absolute percentage different of AC Output Power (%)
R^2 (Actual)	95.6
R^2 (Manufacturer)	100
Error	13.2

2) *Performance of inverter:* The inverter performance can be characterized from its operating efficiency behaviour [17]. In Figure 11, the value of inverter efficiency and the value of nominal AC output power were used for the plot. The actual inverter efficiency was found at 98%. Therefore, the results showed that the inverter was operating near to the rated maximum efficiency during the monitoring period. The efficiency decreased when the AC power generated was below than 10% of the nominal power. In contrast, the maximum efficiency was achieved when the inverter generated AC power more than 10% of the rated nominal output power. Nevertheless, the inverter is operating within its rated values.

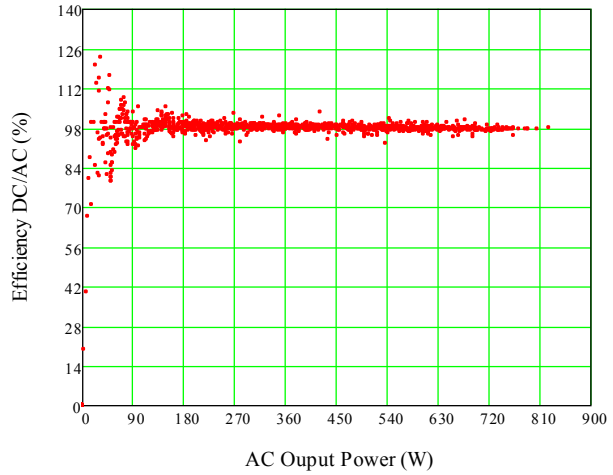

Figure 11 The relationship between the inverter efficiency and AC output power

3) Overall performance of system: Table 9 represents the GCPV system performance for the case study. Overall, the specific yield on the study is observed normal value under Malaysian climate for 8 consecutive days of monitoring. Meanwhile the performance ratio for both actual and manufacturer shows only 65.4% and 74.1% respectively. However, these PR ratio are lower than the standard value of the requirement from SEDA Malaysia in order to proceed on grid [18]. The overall performance has slightly lower than manufacturer predicted due to the factor have discussed above. The diagnostic test has indicated the system is at fault due to aging factor.

Table 9. GCPV System Performance

	Energy Yield (kWh)	**Specific Yield (kWh/kWp)**	**PR (%)**
Actual	35.5	31.7	65.4
Manufacturer	40.2	35.9	74.1

V. CONCLUSIONS

In conclusion, this paper presents the defects and the performance of a grid connected PV system between actual and manufacturer data. The system consists of modules that have been exposed to solar radiation and other environmental conditions for more than 10 years. Defects were described and illustrated. However, as an exception, due to Malaysia climate region with high solar radiation and temperature during the year, due to those extremes suggested it can be related to the defects, faults and degree of degradation. As for coming years, the defects will become extremely noticeable.

ACKNOWLEDGMENT

The authors would like to thank directly and indirectly the Green Energy Research Center, Universiti Teknologi MARA for the necessary information and data available for study and Kementerian Pendidikan Tinggi for the scholarships grant.

REFERENCES

[1] A. R. Gxasheka, E. E. van Dyk, and E. L. Meyer, "Evaluation of performance parameters of PV modules deployed outdoors," *Renew. Energy*, vol. 30, no. 4, pp. 611–620, Apr. 2005.

[2] M. Kottek, J. Grieser, C. Beck, B. Rudolf, and F. Rubel, "World map of the Köppen-Geiger climate classification updated," *Meteorol. Zeitschrift*, vol. 15, no. 3, pp. 259–263, 2006.

[3] M. Z. Hussin, M. H. A. Hamid, Z. M. Zain, and R. A. Rahman, "An evaluation data of solar irradiation and dry bulb temperature at Subang under Malaysian climate," *Proc. - ICSGRC 2010 2010 IEEE Control Syst. Grad. Res. Colloq.*, pp. 55–60, 2010.

[4] M. Z. Hussin, A. M. Omar, Z. M. Zain, and S. Shaari, "Performance of Grid-Connected Photovoltaic System in Equatorial Rainforest Fully Humid Climate of Malaysia," *Int. J. Appl. Power Eng.*, vol. 2, no. 3, pp. 105–114, 2013.

[5] T. Nordmann, L. Clavadetscher, W. G. J. H. M. van Sark, and M. Green, "Analysis of Long - Term Performance of PV Systems," 2014.

[6] M. Köntges, S. Kurtz, C. Packard, U. Jahn, K. A. Berger, K. Kato, T. Friesen, H. Liu, and M. Van Iseghem, "Review on failures of PV modules," 2013.

[7] C. Boonmee, B. Plangklang, and N. Watjanatepin, "System performance of a three-phase PV-grid-connected system installed in Thailand: Data monitored analysis," *Renew. Energy*, vol. 34, no. 2, pp. 384–389, 2009.

[8] L. M. Ayompe, a. Duffy, S. J. McCormack, and M. Conlon, "Measured performance of a 1.72kW rooftop grid connected photovoltaic system in Ireland," *Energy Convers. Manag.*, vol. 52, no. 2, pp. 816–825, Feb. 2011.

[9] A. M. OMAR, S. SHAARI, and S. I. SULAIMAN, *Grid-Connected Photovoltaic Power Systems Design*. Sustainable Energy Development Authority (SEDA) Malaysia.

[10] H. Zainuddin, "Modelling of operating temperature for thin film

modules for free-standing systems in Malaysia," *2013 IEEE Conf. Clean Energy Technol.*, pp. 455–460, 2013.
[11] A. Faranadia, "Prediction of Grid Connected Photovoltaic power systems performance using mathematical approach," *Control Syst. ...*, pp. 13–18, 2014.
[12] S. Djordjevic, D. Parlevliet, and P. Jennings, "Detectable faults on recently installed solar modules in Western Australia," *Renew. Energy*, vol. 67, pp. 215–221, Jul. 2014.
[13] F. Corporation, "Why thermography is good for your business."
[14] E. S. Kopp, V. P. Lonij, A. E. Brooks, P. L. Hidalgo-Gonzalez, and A. D. Cronin, "I-V curves and visual inspection of 250 PV modules deployed over 2 years in tucson," *Conf. Rec. IEEE Photovolt. Spec. Conf.*, pp. 3166–3171, 2012.
[15] S. Chattopadhyay, R. Dubey, V. Kuthanazhi, J. J. John, C. S. Solanki, A. Kottantharayil, B. M. Arora, K. L. Narasimhan, V. Kuber, J. Vasi, A. Kumar, and O. S. Sastry, "Visual degradation in field-aged crystalline silicon PV modules in India and correlation with electrical degradation," *IEEE J. Photovoltaics*, vol. 4, no. 6, pp. 1470–1476, 2014.
[16] E. Kaplani, "Detection of Degradation Effects in Field-Aged c-Si Solar Cells through IR Thermography and Digital Image Processing," *Int. J. Photoenergy*, vol. 2012, pp. 1–11, 2012.
[17] R. A. Rahman, S. I. Sulaiman, A. M. Omar, S. Shaari, and Z. M. Zain, "Performance analysis of a grid-connected PV system at malaysian energy centre, Malaysia," *PEOCO 2010 - 4th Int. Power Eng. Optim. Conf. Progr. Abstr.*, pp. 480–483, 2010.
[18] "SEDA PORTAL." [Online]. Available: http://seda.gov.my/. [Accessed: 02-Dec-2015].